

All-passive microwave-diode nonreciprocal metasurface

Xiaozhen Yang ¹, Erda Wen^{1,2} & Daniel Sievenpiper^{1,2}

Breaking reciprocity in the microwave frequency range is strongly desirable in the development of modern electronic systems, as it enables nonreciprocal wave absorbing, non-reciprocal beam steering, frequency conversion, and protection of sensitive devices from high energy sources. However, the typical approaches involve bulky biasing magnets or complex spatial-temporal modulations. As such, resorting to lightweight and all-passive platforms would result in optimal configurations and efficient integration. Starting from a circuit model, we theoretically demonstrate the nonreciprocal behavior on a transmission line building block creating a strong field asymmetry with a switchable matching stub to enable two distinct working states. After translating to an electromagnetic model, this concept is first proved by simulation and then experimentally verified on a microstrip-line-based diode-integrated metasurface showing nonreciprocal transmission. This printed circuit board design is expected to find various applications in electromagnetic protecting layers, communication systems, microwave isolators and circulators.

¹Electrical and Computer Engineering Department, University of California, San Diego, 9500 Gilman Dr., La Jolla 92093 CA, USA. ²These authors contributed equally: Erda Wen, Daniel Sievenpiper. ✉email: xiy003@eng.ucsd.edu

Reciprocity is a fundamental property of non-magnetic, passive, linear and time-invariant systems, which states that the transmission from the source to the observation point remains the same if their locations are interchanged. In the past decades, with the fast development in acoustics¹, electromagnetism^{2,3}, optics^{4,5}, and electronics⁶, breaking the transmission symmetry becomes a crucial task for various applications, from optical isolation to wireless communication^{7–10}. In the microwave regime^{11,12}, nonreciprocal metasurfaces raise growing interests because they provide a compact, ultra-thin, lightweight platform to manipulate waves in a unidirectional manner, which enables nonreciprocal wave absorbing, non-reciprocal beam steering, frequency conversion, and consequently can be used to protect sensitive devices from high energy sources^{9,13–15}.

The conventional approach to break reciprocity in electro-magnetism relies on ferrite material, such as yttrium iron garnet and iron oxide with other metallic elements, which exhibits the Faraday effect^{16,17}. While the Faraday rotation enables the functionality of optical isolators and circulators, polarization rotations might not be preferred in wireless communication systems (especially for linear polarization, maintaining the polarization state of the transmitted signals is essential, unnecessary polarization mismatch occurs if the linear polarization is rotated which results in lower transmission rate and signal to noise ratio). Besides, ferrites are expensive compared to printed circuit board designs. It is bulky and brittle in large-scale applications and incompatible with modern lightweight and compact integrated circuits devices. In addition, external magnetic bias is typically needed for ferrite-based designs^{18,19}.

Recent research proposes to violate the fundamental assumption of the Lorentz reciprocity theorem to break the transmission symmetry by employing spatial-temporal modulation, active elements or nonlinearity^{1–3}. However, such modulation strategy usually requires a controlling system which needs an additional power supply^{15,20–23}. In addition, some works adopt active electronic elements, including transistor-based amplifiers/switches and varactors to break the reciprocity^{10,24–26}. Although modulation is absent, those designs still require a biasing circuit. Another concern is that these approaches require a large biasing/modulation signal under high power incident such that the biasing/modulation signal overwhelms the RF signal. Nonlinearity, on the other hand, provides an alternative to engineer all-passive

nonreciprocal devices. Material with strong Kerr nonlinearity has been proven to be a good candidate for nonreciprocal optical devices, including circulators and isolators, if the structure is designed to have field asymmetry when illuminated from opposite directions^{7,27–30}.

However, other types of nonlinearity need to be implemented as a counterpart to the electro-optic effect in microwave frequencies to develop an all-passive, magnetic-free nonreciprocal structure. Ref. ³¹ adopts an asymmetrical structure and resonators loaded with an imaginary lumped component, whose capacitance varies with continuous AC signals, to imitate the Kerr effect, such that the resonance frequency shifts differently for waves propagating in opposite directions. An experimental work in microwave circuits proved this concept by adopting varactors to introduce a frequency shift to resonators in the megahertz range³². However, this approach can not be scaled to higher frequencies since the varactors are infeasible due to their high loss.

Here, we propose a feasible all-passive nonreciprocal metasurface design without any biasing based on a microstrip line (MSL) with the integration of accessible nonlinear elements, Schottky diodes, to break the transmission symmetry. The simplicity of this model allows fast design in a circuit model by treating the MSL as an ideal transmission line (TL), which makes this method more appealing. The field asymmetry directly originates from the impedance contrast of the MSL, which is later proven to be the determining parameter of the nonreciprocity. The Schottky diodes connect a matching stub to the ground plane, and the field intensity at their location differs significantly for waves propagating in opposite directions. Thus, the matching stub is either open or shorted depending on the incidence direction, which further determines the transmission. In this article, we extend the MSL structure to a three-layered metasurface with low transmission in one direction while allowing wave propagation from the opposite direction, which resembles the diode behavior. Immune to Faraday rotation, it is potentially applicable in various scenarios including protecting radar or communication systems against high power microwave sources, without using conventional EM circulators and isolators. Since modulation is absent, this design can be scaled to other frequencies, while time-modulated design is limited due to the difficulty of fast modulation at higher frequencies and the response time of the modulated components. In addition, it is more universally applicable when a bias is inaccessible.

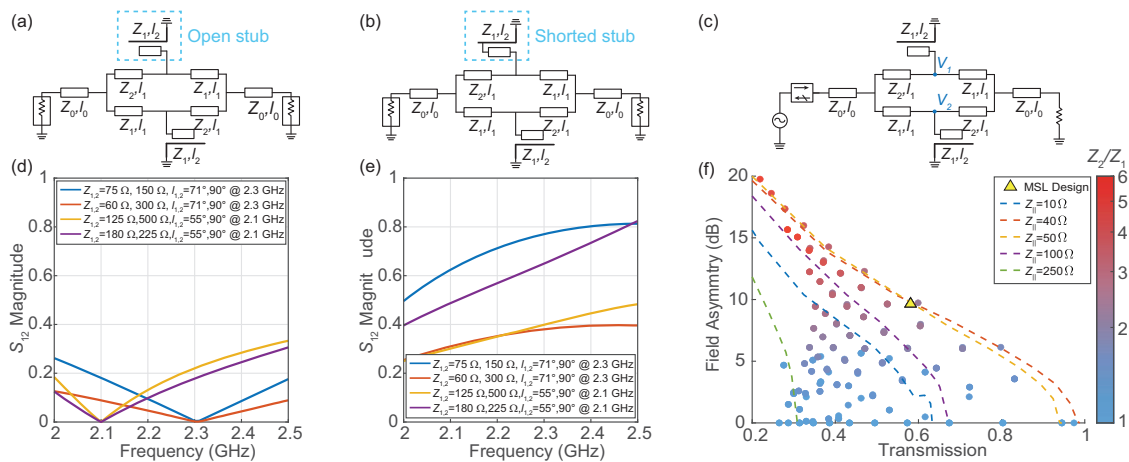


Fig. 1 Ideal transmission line models. $Z_0 = 50 \Omega$. Z_1 and Z_2 are the characteristic impedance of the transmission line branches. **a** OFF state (diodes not triggered, open stub) circuit model. **b** ON state (diodes triggered, shorted stub) circuit model. **c** Transient simulation model in OFF state. **d** Transmission in the OFF state. **e** Transmission in the ON state. **f** Trade-off between field asymmetry and the ON state transmission with $l_1 = 71^\circ$, $l_2 = 90^\circ$ at 2.3 GHz. The color of the dots represent the impedance contrast defined by Z_2/Z_1 .

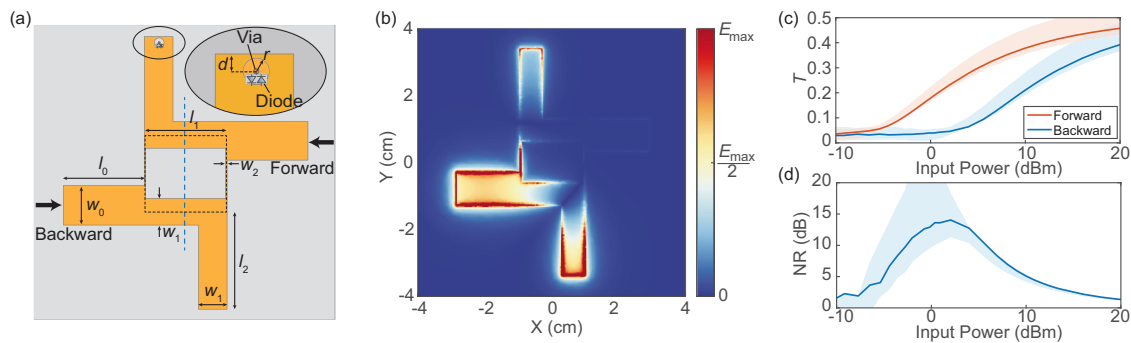


Fig. 2 Microstrip line model. **a** Illustration of microstrip line translating from the yellow triangle in Fig. 1f. The width of the microstrip line $w_{0,1,2}$, corresponds to characteristic impedance $Z_{0,1,2} = 50, 66, 200 \Omega$. **b** Field distribution in the OFF state under backward incidence at 2.3 GHz. The color indicates the electric field strength. **c** The simulated transmission rate (T) under different propagation directions. Red line: forward incidence for 2.05 GHz. Blue line: backward incidence for 2.05 GHz. Red shaded area: forward incidence from 2.03 GHz to 2.15 GHz. Blue shaded area: backward incidence from 2.03 GHz to 2.15 GHz. **d** The simulated nonreciprocity (NR). Blue line: 2.05 GHz. Blue shaded area: 2.03 GHz to 2.15 GHz.

Results

Transmission line design. Nonlinear devices are defined by their power-dependent behavior. Thus when the field distribution changes between one incident direction and the opposite, placing a nonlinear component at the field asymmetrical location enables the whole system to be nonreciprocal. Take the ideal diode for instance, the ON and OFF working states are determined by the local field intensity and induce two distinct operating states of the system for different transmission/absorption due to the change of its topology. The nonreciprocity is maximized when deploying the diodes at the strongest asymmetry point. Then, a non-reciprocal metasurface can be developed by simply folding this building block and separating the two halves by a ground plane with antennas connected to receive and transmit signals.

The proposed TL model that creates and utilizes a field asymmetry is illustrated in Fig. 1. Starting with the ideal circuit model, two different impedances, Z_1 and Z_2 , are chosen to create the field asymmetry at the end of the matching stub. Nonreciprocity is then achieved by integrating diodes on the upper stub. As a proof of concept, we simplified the nonlinear power-dependent behavior of the diodes to two static states so that the matching stub is either an open (the OFF state, Fig. 1a) or a shorted stub (the ON state, Fig. 1b) depending on the field intensity under different incident directions, while the lower stub is always open. When it is shorted, better matching occurs, resulting in higher transmission. Otherwise, it has lower transmission rate. Since the state of the upper matching stub is determined by the field intensity, a stronger asymmetry in field distribution is crucial for achieving higher nonreciprocity.

To analyze the field asymmetry of this TL design, we performed S parameter and transient simulations in Advanced Design System (ADS) to study the static states behavior. The field asymmetry is defined by the ratio of voltage at two observation points, V_1 and V_2 in Fig. 1c as $20 \log_{10}(\frac{V_2}{V_1})$. Although the diode is located at the end of the matching stub, it is reasonable to approximate the ratio of the field intensity at that location by these observation points. The transmission rate for the static states are studied by S parameter simulation as in Fig. 1d and e. The length of the matching stub, L_2 , determines the operating frequency which has the highest field asymmetry. The minimum transmission occurs at the frequency when the electrical length of the matching stub is $\lambda/4$ in the OFF state, since the waves are shorted by the matching stub, as shown in Fig. 1d. For the ON state, since one matching stub is shorted, higher transmission is observed as illustrated in (e). L_1 does not affect the overall performance here since only an ideal TL is involved, but it should

be chosen properly in a real electromagnetic (EM) design to follow the TL principles. The field asymmetry is dominated by impedance contrast between Z_1 and Z_2 . By examining different impedance values and contrast for $50 \Omega \leq Z_1 \leq Z_2 \leq 500 \Omega$, a trade-off between field asymmetry and the ON state transmission is observed in Fig. 1f³³. All the data in (f) is simulated with $l_1 = 71^\circ$, $l_2 = 90^\circ$ at 2.3 GHz. The color in (f) represents the impedance contrast defined by $\frac{Z_2}{Z_1}$. Warm-colored dots are concentrated on the upper-left corner and the cold-colored ones are scattered at the bottom, demonstrating the trade-off relationship between impedance contrast and field asymmetry. In addition, all data points are gathered in the lower-left half and is bounded by $Z_{||} = 50 \Omega$, where $\frac{1}{Z_{||}} = \frac{1}{Z_1} + \frac{1}{Z_2}$, which proves the trade-off between field asymmetry and transmission. Higher impedance contrast does create stronger field asymmetry, but the discontinuities and reflections largely undermines the transmission rate. Thus, the upper limit scenario occurs when avoiding the unnecessary reflections due to mismatch. As expected, the field distribution is completely symmetrical if $Z_1 = Z_2$.

Microstrip line design. To transform the ideal circuit model to a feasible electromagnetic prototype, we adopt a MSL which can be easily fabricated and integrated to printed circuit board (PCB) designs. Fig. 2a illustrates a MSL design with a reasonable field asymmetry and transmission rate at the upper limit of the trade-off relation, shown as the yellow triangle in Fig. 1f. The impedance of Z_1 and Z_2 is 66 Ω and 200 Ω , respectively. The length of the matching stub is l_2 determines the center frequency to be around 2.3 GHz. l_1 should be as short as possible to shrink the size, but not to short to still behave as a TL. The thickness of the substrate is chosen such that the width of a 200 Ω MSL can be precisely manufactured. A pair of oppositely oriented diodes are required to react to sinusoidal waves. Incidence from the right-hand side is defined as forward propagation and excitation from the opposite side is called backward propagation.

The static field distribution in the OFF state is illustrated in Fig. 2b under backward excitation. Since this structure has 180° rotational symmetry, the forward field distribution can be obtained by rotating that of the backward by 180°. That is to say the field asymmetry at the location of the diode can be seen as the ratio between the upper stub and the lower stub under forward or backward incidence. The transmission rate for static forward and backward propagation is 0.65 and 0.09 at 2.3 GHz, and the field asymmetry is 8.3 dB, which agrees well with the circuit model.

This structure is further studied using EM-circuit co-simulation to verify its power-dependent nonreciprocal behavior with the integration of a real Schottky diode for fast response. Power-related nonreciprocal transmission is observed from 2.03 GHz to 2.15 GHz with more than 10 dB nonreciprocity as shown in Fig. 2c and d. Frequency shift is inevitable due to the integration of real diodes. Here, the transmission (T) is the voltage ratio between the received and the transmitted, and the nonreciprocity is defined by

$$\text{NR} = 20\log_{10}\left(\frac{T_+}{T_-}\right), \quad (1)$$

where T_{\pm} denotes the forward and backward transmission rate. The incident power is calculated by $\frac{V_{\text{tran}}^2}{2Z_0}$, where V_{tran} is the amplitude of the voltage source. The system is reciprocal under low-power illumination since the diodes are not triggered. As the power increases, the nonreciprocity rises because the diodes are only turned on under forward incidence and it reaches the maximum when the voltage across the diodes of backward excitation is close to the threshold of the diodes. The transmission rate finally converges as the incident power continues increasing, since the threshold of the diodes become negligible compared with the voltage cross the diodes. More than 10 dB nonreciprocity is achieved between -2.8 dBm and 5.6 dBm incidence for 2.05 GHz. The dynamic range of the proposed design is adjustable by varying the impedance contrast. An example is given in the Supplementary Note 2 and Supplementary Fig. 3 with larger dynamic range by increasing $\frac{Z_2}{Z_1}$. Note that the width of the transmission line should be considered for easy fabrication. The static states and power-dependent nonreciprocal performance is further demonstrated through measurement and the results are included in Supplementary Note 1 and Supplementary Fig. 1, which proves its potentiality as a building block of EM isolators and circulators.

Metasurface design and measurement. After demonstrating the nonreciprocity of the MSL through simulations and measurements, we extend it to a metasurface as illustrated in Fig. 3a, which can be used to protect sensitive devices from high power sources while allowing one-way communication. This is attained by folding the MSL structure and separating the two halves on

two layers with a ground plane in between as illustrated in Fig. 3b. These MSL layers are connected by two vias through the holes on the central ground plane. Two patch antennas are attached to the MSL to receive and transmit the EM signals. Since the patch antenna only supports linear polarization in the Z direction, all the following results are the outcome under Z-polarization illumination. The simulated results for the orthogonal polarization in X direction is shown in Supplementary Note 3 and Supplementary Fig. 4, showing zero transmission rate for both propagation directions.

The performance of this design is studied using EM-circuit co-simulation on a unit cell with periodic boundaries to reduce the computational cost. Since the excitation is free space waves, the definition of input power is different than that in the MSL simulations, where the incident is calculated by the voltage between the MSL and ground plane. Here, the input refers to the power over the area of one unit cell. Similar to the MSL structure, a nonreciprocal transmission with the same trend is observed as shown in Fig. 3c and d. The bandwidth of this unit cell is narrowed down to 2.18 GHz to 2.25 GHz due to the patch antenna.

A 6 by 3-unit prototype, as shown in Fig. 4c, is fabricated to measure its nonreciprocity. This experiment is conducted in an anechoic chamber, as in Fig. 4b, to minimize the effect from the environment. To avoid diffraction and to confine energy propagation, the surface is placed inside a parallel plate TEM waveguide with the same height as illustrated in Fig. 4a. Microwave absorbers are placed at the top and the bottom of the waveguide to further reduce diffraction. The incident signal is generated by a vector network analyzer (VNA), amplified by a power amplifier and transmitted by a horn antenna. After propagating through the surface, the signal is received by another horn antenna connected to the VNA. Note that the input power here has the same definition as in Fig. 3c and d, referring to the the power incident on each unit cell. Having the setup fixed, the backward transmission is measured by flipping the sample. In addition to the forward and backward transmission scenarios, we also measured the transmission of a blank waveguide (the blank case), representing the total incident power, and the diffraction from the sides with an equal size aluminum sheet (the PEC case). Although the waveguide is wider than the sample, the diffraction measured under the PEC case is 30 dB less than that of the blank

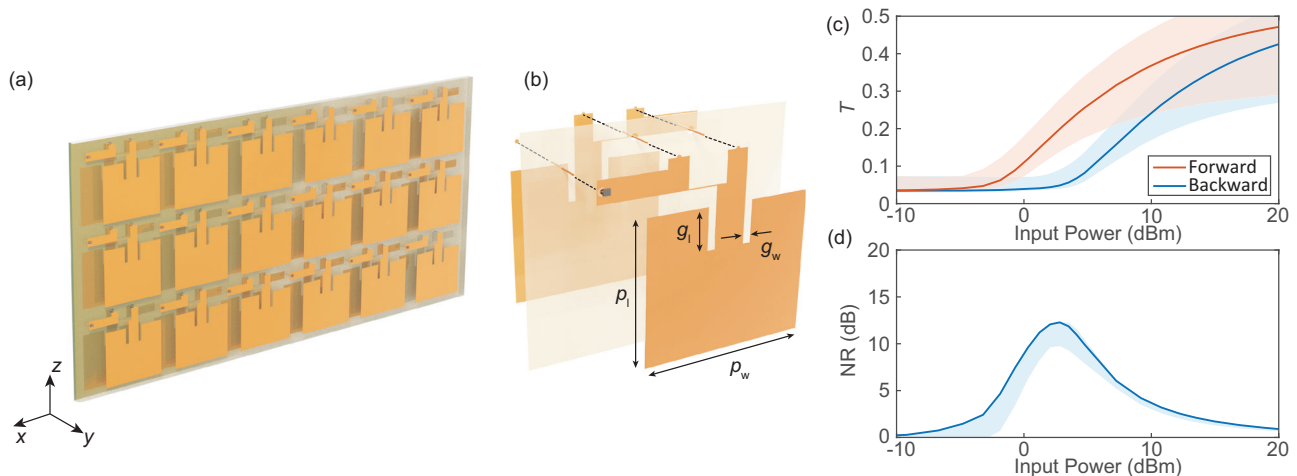


Fig. 3 Metasurface design. **a** Illustration of a 6 by 3-unit surface. **b** A detailed illustration of the three-layer layout. p_l and p_w are the length and width of the patch antenna, respectively. g_l and g_w are the length and width of the matching slot on the patch antenna. **c** The simulated transmission rate (T) under different propagation directions. Red line: forward incidence for 2.21 GHz. Blue line: backward incidence for 2.21 GHz. Red shaded area: forward incidence from 2.18 GHz to 2.25 GHz. Blue shaded area: backward incidence from 2.18 GHz to 2.25 GHz. **d** The simulated nonreciprocity (NR). Solid line: 2.21 GHz. Shaded area: 2.18 GHz to 2.25 GHz.

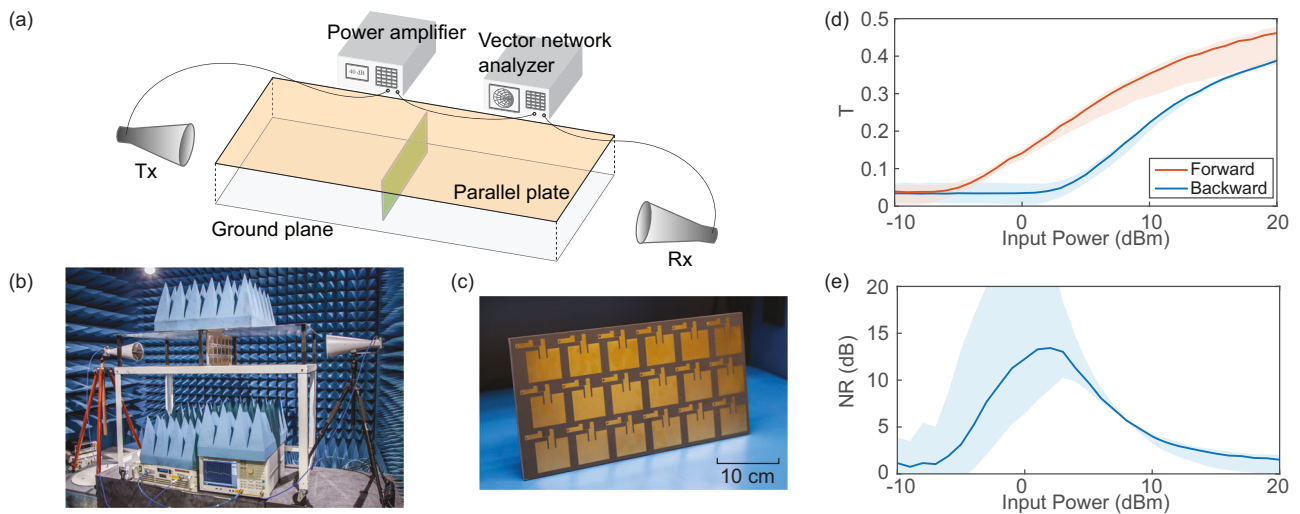


Fig. 4 Measurement inside a TEM waveguide to reduce diffraction. **a** Illustration of measurement setup. **b** Picture of measurement setup. **c** Picture of the prototype. **d** The measured transmission rate (T) under different propagation direction. Red line: forward incidence for 2.05 GHz. Blue line: backward incidence for 2.05 GHz. Red shaded area: forward incidence from 2.02 GHz to 2.06 GHz. Blue shaded area: backward incidence from 2.02 GHz to 2.06 GHz. **e** The measured nonreciprocity (NR). Solid line: 2.05 GHz. Shaded area: 2.02 GHz to 2.06 GHz.

case, which is negligible. Thus, it is reasonable to assume that no diffraction occurs in this measurement. The transmission in the measurement is defined by

$$T_{\pm} = \sqrt{\frac{P_{\pm}}{P_{\text{blk}}}}, \quad (2)$$

where $P_{\pm/\text{blk}}$ is the absolute power received by Rx measured with board under forward/backward propagation and the blank case. The nonreciprocity is still defined by Eq. (1). The measurement results are shown in Fig. 4d and e, similar to the simulation results in Fig. 3, a nonreciprocal transmission behavior is observed under different incident directions. More than 10 dB isolation is achieved between -1.8 dBm to 4.7 dBm at 2.05 GHz.

Discussion

We proposed a MSL-based all-passive nonreciprocal metasurface by applying nonlinear devices at field asymmetrical locations, and verified its “diode”-like one-way behavior under opposite incident directions through experiments. Unlike the Kerr effect approach in photonic systems, where the nonlinearity originates from the material, this method is rather general in the microwave regime. Since the field asymmetry comes from the metallic topology, the substrate is free of choice. The option for diodes are also numerous in various packages, material and arrangement. Moreover, it can be scaled to other frequencies, and it is rather easy to modify the input and output impedance by adjusting the width of the MSL. In addition, the working range of power is adjustable using different arrangements of diodes, which is equivalent to adopting diodes with different threshold voltages (see Supplementary Note 2 and Supplementary Fig. 2). Different from the ferrite approach, its immunity to Faraday rotation makes it more appealing for communication systems. Different polarizations can be achieved using other types of antennas, or modifying the feeding point of the current design if polarization conversion is preferred. This lightweight, low-profile and low-cost PCB design is promising in various applications, including EM protecting layers such as radomes and nonreciprocal absorbing material, and EM isolators and circulators by cascading the MSL structure. We realize this design is subject to the limitation of dynamic reciprocity that small signals lose nonreciprocity in the

presence of large signals³⁴, since the nonreciprocity is induced by field intensity which is the summation of all signals.

Methods

Fabrication. The MSL structure is manufactured on a 3.175 mm thick 8.5 cm by 8.5 cm double-sided Duroid Rogers 5880 PCB with coaxial feed. The dimensions are $w_{0,1,2} = 9.7, 6.63, 0.31$ mm, $l_{0,1,2} = 1.9, 1.9, 2.4$ cm, $d = 1.4$ mm, $r = 1.2$ mm, and the radius of the vias are 10 mil. The center of the 66 Ω and 200 Ω MSL forms a square whose side length is l_1 shown as the black dotted line in Fig. 2a. The Schottky diode used in the EM-circuit co-simulation is BAT15-04W. There is a hole on the upper matching stub to place the diodes to connect the stub to the ground plane through a via in the ON state. The metasurface is fabricated on a three-layer 42.3 cm by 20.5 cm Duroid Rogers 5880 PCB, both of cores are 3.175 mm in thickness. The dimensions for the patch antenna, resonating at 2.19 GHz, are $p_w = 53.87$ mm, $p_l = 45$ mm, $g_w = 2.5$ mm, $g_l = 13$ mm. Note that the periodicity in y and z direction is 6.8 cm and 6.6 cm, respectively, to avoid overlapping of the top and bottom layer for a through via.

EM-circuit co simulation. After simulating the EM structure from DC to 8 GHz, we extract its S parameters and perform transient simulation in circuit with the diodes SPICE model provided by the manufacturer. The metasurface is simulated under periodic boundaries using unit cell. Studies of third order harmonics, third-order intermodulation product and 1-dB compression point is included in Supplementary Note 4 and Supplementary Figs. 5–8, which show that the harmonics are negligible under all incident power and that the defined 1-dB compression point is out of the 10 dB nonreciprocity range.

Measurement. The TEM waveguide is 120 cm long, 60 cm wide and its height is 20.3 cm, which is the same as the prototype. The distance between the edge of the horn antenna (Rx) and the TEM waveguide is 10 cm, which excites plane wave inside the waveguide. Devices involved: VNA, Keysight E5071C, power amplifier Ophir 5022, Tx and Rx RCDLPHA2G18B. Due to the involvement of an amplifier, instead of S parameters, the VNA is always measuring the absolute power on Rx. To measure under different incident power, the input power of the VNA varies from -40

dBm to -10 dBm with the amplifier providing a 30 dB amplification. All the data is averaged by 8 times, and the devices are controlled by Python.

Data availability

All relevant data is available on [figshare](https://figshare.com) or from the corresponding author upon request.

Received: 13 May 2023; Accepted: 2 November 2023;

Published online: 21 November 2023

References

- Nassar, H. et al. Nonreciprocity in acoustic and elastic materials. *Nat. Rev. Mater.* **5**, 667–685 (2020).
- Caloz, C. et al. Electromagnetic nonreciprocity. *Phys. Rev. Appl.* **10**, 047001 (2018).
- Kord, A., Sounas, D. L. & Alu, A. Microwave nonreciprocity. *Proc. IEEE* **108**, 1728–1758 (2020).
- Shoji, Y., Miura, K. & Mizumoto, T. Optical nonreciprocal devices based on magneto-optical phase shift in silicon photonics. *J. Opt.* **18**, 013001 (2015).
- Kutsaev, S. V. et al. Up-and-coming advances in optical and microwave nonreciprocity: From classical to quantum realm. *Adv. Photonics Res.* **2**, 2000104 (2021).
- Reiskarimian, N. A review of nonmagnetic nonreciprocal electronic devices: Recent advances in nonmagnetic nonreciprocal components. *IEEE Solid-State Circuits Mag.* **13**, 112–121 (2021).
- Xu, X.-W., Li, Y., Li, B., Jing, H. & Chen, A.-X. Nonreciprocity via nonlinearity and synthetic magnetism. *Phys. Rev. Appl.* **13**, 044070 (2020).
- Kong, C., Xiong, H. & Wu, Y. Magnon-induced nonreciprocity based on the magnon kerr effect. *Phys. Rev. Appl.* **12**, 034001 (2019).
- Zhang, L. et al. Breaking reciprocity with space-time-coding digital metasurfaces. *Adv. Mater.* **31**, 1904069 (2019).
- Popa, B.-I. & Cummer, S. A. Non-reciprocal and highly nonlinear active acoustic metamaterials. *Nat. Commun.* **5**, 1–5 (2014).
- Pozar, D. M. *Microwave engineering*. (John Wiley & Sons, New York, 2011).
- Balanis, C. A. *Advanced engineering electromagnetics*. (John Wiley & Sons, NJ, 2012).
- Sievenpiper, D., Zhang, L., Broas, R. F., Alexopolous, N. G. & Yablonovitch, E. High-impedance electromagnetic surfaces with a forbidden frequency band. *IEEE Trans. Microw. Theory Tech.* **47**, 2059–2074 (1999).
- Sievenpiper, D. F., Schaffner, J. H., Song, H. J., Loo, R. Y. & Tansonan, G. Two-dimensional beam steering using an electrically tunable impedance surface. *IEEE Trans. Antennas Propag.* **51**, 2713–2722 (2003).
- Li, A. et al. Time-modulated nonreciprocal metasurface absorber for surface waves. *Opt. Lett.* **45**, 1212–1215 (2020).
- Fuller, A. B. *Ferrites at microwave frequencies*. (IET, London, 1987).
- Adam, J. D., Davis, L. E., Dionne, G. F., Schloemann, E. F. & Stitzer, S. N. Ferrite devices and materials. *IEEE Trans. Microw. theory Tech.* **50**, 721–737 (2002).
- Apaydin, N., Sertel, K. & Volakis, J. L. Nonreciprocal leaky-wave antenna based on coupled microstrip lines on a non-uniformly biased ferrite substrate. *IEEE Trans. Antennas Propag.* **61**, 3458–3465 (2013).
- Parsa, A., Koderia, T. & Caloz, C. Ferrite based non-reciprocal radome, generalized scattering matrix analysis and experimental demonstration. *IEEE Trans. Antennas Propag.* **59**, 810–817 (2010).
- Dinc, T. et al. Synchronized conductivity modulation to realize broadband lossless magnetic-free non-reciprocity. *Nat. Commun.* **8**, 1–9 (2017).
- Cardin, A. E. et al. Surface-wave-assisted nonreciprocity in spatio-temporally modulated metasurfaces. *Nat. Commun.* **11**, 1–9 (2020).
- Yang, X., Wen, E. & Sievenpiper, D. F. Broadband time-modulated absorber beyond the bode-fano limit for short pulses by energy trapping. *Phys. Rev. Appl.* **17**, 044003 (2022).
- Nagulu, A. et al. Chip-scale floquet topological insulators for 5g wireless systems. *Nat. Electron.* **5**, 300–309 (2022).
- Reiskarimian, N. & Krishnaswamy, H. Magnetic-free non-reciprocity based on staggered commutation. *Nat. Commun.* **7**, 1–10 (2016).
- Taravati, S., Khan, B. A., Gupta, S., Achouri, K. & Caloz, C. Nonreciprocal nongyrotropic magnetless metasurface. *IEEE Trans. Antennas Propag.* **65**, 3589–3597 (2017).
- Chapman, B. J. et al. Widely tunable on-chip microwave circulator for superconducting quantum circuits. *Phys. Rev. X* **7**, 041043 (2017).
- Fan, L. et al. An all-silicon passive optical diode. *Science* **335**, 447–450 (2012).
- Jin, B. & Argyropoulos, C. Self-induced passive nonreciprocal transmission by nonlinear bifacial dielectric metasurfaces. *Phys. Rev. Appl.* **13**, 054056 (2020).
- Yang, K. Y. et al. Inverse-designed non-reciprocal pulse router for chip-based lidar. *Nat. Photonics* **14**, 369–374 (2020).
- Mekawy, A., Sounas, D. L. & AlÜ, A. Free-space nonreciprocal transmission based on nonlinear coupled fano metasurfaces. *Photonics*, **8**, 139 (2021).
- Mahmoud, A. M., Davoyan, A. R. & Engheta, N. All-passive nonreciprocal metastructure. *Nat. Commun.* **6**, 1–7 (2015).
- Sounas, D. L., Soric, J. & Alu, A. Broadband passive isolators based on coupled nonlinear resonances. *Nat. Electron.* **1**, 113–119 (2018).
- Sounas, D. L. & AlÜ, A. Fundamental bounds on the operation of fano nonlinear isolators. *Phys. Rev. B* **97**, 115431 (2018).
- Shi, Y., Yu, Z. & Fan, S. Limitations of nonlinear optical isolators due to dynamic reciprocity. *Nat. Photonics* **9**, 388–392 (2015).

Acknowledgements

This work is supported by Office of Naval Research under Grant No. N0014-20-1-2710.

Author contributions

X.Y. proposed the concept and performed the simulations and analysis under the supervision of D.F. X.Y. and E.W. performed the measurement and generated all figures. X.Y. wrote the manuscript, with inputs from E.W. and D.F.

Competing interests

The authors declare no competing interests.

Additional information

Supplementary information The online version contains supplementary material available at <https://doi.org/10.1038/s42005-023-01445-0>.

Correspondence and requests for materials should be addressed to Xiaozhen Yang.

Peer review information *Communications Physics* thanks Alex Krasnok, Aravind Nagulu and the other, anonymous, reviewer(s) for their contribution to the peer review of this work. A peer review file is available.

Reprints and permission information is available at <http://www.nature.com/reprints>

Publisher's note Springer Nature remains neutral with regard to jurisdictional claims in published maps and institutional affiliations.

 **Open Access** This article is licensed under a Creative Commons Attribution 4.0 International License, which permits use, sharing, adaptation, distribution and reproduction in any medium or format, as long as you give appropriate credit to the original author(s) and the source, provide a link to the Creative Commons license, and indicate if changes were made. The images or other third party material in this article are included in the article's Creative Commons license, unless indicated otherwise in a credit line to the material. If material is not included in the article's Creative Commons license and your intended use is not permitted by statutory regulation or exceeds the permitted use, you will need to obtain permission directly from the copyright holder. To view a copy of this license, visit <http://creativecommons.org/licenses/by/4.0/>.

© The Author(s) 2023